ISSN 2176-5480

22nd International Congress of Mechanical Engineering (COBEM 2013)
November 3-7, 2013, Ribeirão Preto, SP, Brazil

LONGITUDINAL STABILITY ANALYSIS OF A HYPERSONIC AIRBREATHING VEHICLE

Giannino Ponchio Camillo *
Instituto Tecnológico de Aeronáutica (ITA/DCTA)
giannino@ieav.cta.br
* *Research Engineer at Instituto de Estudos Avançados (IEAv/DCTA)*
Fabio Andrade de Almeida
Instituto de Aeronáutica e Espaço (IAE/DCTA)
almeidafaa@iae.cta.br

Abstract. *Hypersonic airbreathing flight is among the most prominent technologies regarding aerospace applications currently under research around the globe. Brazil's Institute for Advanced Studies (IEAv/DCTA) is conducting studies in this area aiming at satellite launching, with the 14-X Aerospace Hypersonic Vehicle as study platform. One of the paramount challenges in such high-speed flights is stability and control. This paper presents an initial longitudinal stability study of a simplified rigid hypersonic vehicle. This vehicle is a two-dimensional representation of the 14-X, comprising both the airframe and the SCRAMJET system. The aerodynamic loads are obtained using two-dimensional shock and expansion theory, and the engine is assumed to be turned off during the analysis. No active control systems are considered. Newtonian-based six-degree-of-freedom equations of motion are presented, considering a spherical, rotating Earth, and hypersonic flight is simulated using MATLAB® Simulink to enlighten free-flight stability issues.*

Keywords: *hypersonic flight, 14-X, Longitudinal stability*

1. INTRODUCTION

The Institute for Advanced Studies (IEAv/DCTA) is conducting studies in the field of hypersonic airbreathing flight with the objective of satellite launching. The main study platform for such studies is the 14-X Aerospace Hypersonic Vehicle, first presented in the work of Rolim (2009). The 14-X Aerospace Hypersonic Vehicle is a cone-based waverider (responsible for lift generation) with integrated SCRAMJET (thrust generation). This thrust mechanism is only operable at supersonic speeds. An auxiliary thrust system is needed to boost the vehicle to operating conditions.

In this paper, stability issues regarding the longitudinal flight of a bidimensional simplification of the 14-X are addressed. The simplified 14-X, called 14-XB, presents a purely bidimensional geometry, obtained by laterally extruding the central longitudinal cross-section of the original 14-X. An all-moving horizontal tail is designed in order to stabilize the vehicle during flight. Figure 1 shows the 14-XB concept with all-moving horizontal tail.

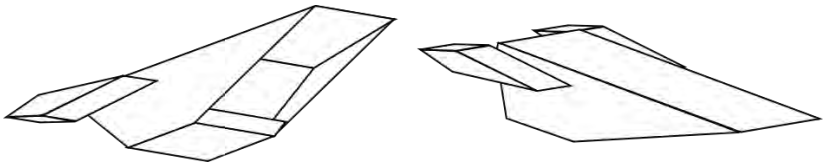

Figure 1. 14-XB concept

In this first study, free-flight is considered, meaning that the horizontal tail must be designed in a fashion such as no active control should be required to further stabilize the aircraft. If possible, this is the most desirable solution for a first vehicle flight test.

In the next sections the aerodynamics and flight dynamics equations used to design the all-moving horizontal tail and simulate a free-flight with spherical, rotating Earth are presented. The aircraft is then trimmed and subjected to a free-flight using both rotating and non-rotating Earth equations, and results are compared and discussed.

2. PROBLEM FORMULATION

2.1 Aerodynamics

A mathematical model that properly represents the physical phenomena that take place along this vehicle was obtained using basic supersonic flow theory, assuming calorically perfect gas, as given by Anderson (1990), following the approach to the aerodynamics formulation used by Austin (2002) and Frendreis *et al.*(2009).

ISSN 2176-5480

Equation (1) shows the correlation between flow deflection angle, shock wave angle and flow Mach number for a bidimensional supersonic flow.

$$tan\theta = 2cot\beta\left[\frac{M_1^2 sin^2\beta - 1}{M_1^2(\gamma + cos2\beta) + 2}\right] \quad (1)$$

Knowing these values, flow density, pressure, temperature and Mach number after the shock wave are easily calculated using Eqs. (2) – (7).

$$M_{n1} = M_1 sin\beta \quad (2)$$

$$\frac{\rho_2}{\rho_1} = \frac{(\gamma+1)M_{n1}^2}{(\gamma-1)M_{n1}^2+2} \quad (3)$$

$$\frac{p_2}{p_1} = 1 + \frac{2\gamma}{\gamma+1}(M_{n1}^2 - 1) \quad (4)$$

$$\frac{T_2}{T_1} = \frac{p_2}{p_1}\frac{\rho_1}{\rho_2} \quad (5)$$

$$M_{n2}^2 = \frac{M_{n1}^2 + [2/(\gamma-1)]}{[2\gamma/(\gamma-1)]M_{n1}^2 - 1} \quad (6)$$

$$M_2 = \frac{M_{n2}}{sin(\beta-\theta)} \quad (7)$$

If the flow deflection angle is negative (representing an expansion), Prandtl-Meyer expansion theory can be used to determine flow properties (Anderson, 1990). Expansion is assumed to be isentropic, and flow properties are given by Eqs. (8) – (11).

$$\theta = \nu(M_2) - \nu(M_1) \quad (8)$$

$$\nu(M) = \sqrt{\frac{\gamma+1}{\gamma-1}}\ \tan^{-1}\sqrt{\frac{\gamma+1}{\gamma-1}(M^2-1)} - \tan^{-1}\sqrt{M^2-1} \quad (9)$$

$$\frac{T_1}{T_2} = \frac{1+\frac{\gamma-1}{2}M_2^2}{1+\frac{\gamma-1}{2}M_1^2} \quad (10)$$

$$\frac{p_1}{p_2} = \left[\frac{1+\frac{\gamma-1}{2}M_2^2}{1+\frac{\gamma-1}{2}M_1^2}\right]^{\frac{\gamma}{\gamma-1}} \quad (11)$$

If the expansion is confined (such as in the vehicle combustion chamber and nozzle), Mach wave reflection must be taken into account, and the flow properties can be calculated by area relation (Heiser and Pratt, 1994), assuming constant total properties, Eqs. (12) – (14).

$$\frac{A_2}{A_1} = \frac{M_1}{M_2}\left[\frac{1+\frac{\gamma-1}{2}M_2^2}{1+\frac{\gamma-1}{2}M_1^2}\right]^{\frac{\gamma+1}{2(\gamma-1)}} \quad (12)$$

$$\frac{T_0}{T} = 1 + \frac{\gamma-1}{2}M^2 \quad (13)$$

$$\frac{p_0}{p} = \left(1 + \frac{\gamma-1}{2}M^2\right)^{\frac{\gamma}{\gamma-1}} \quad (14)$$

2.2 Flight Dynamics

Flight dynamics are governed by equations largely explored in the literature (Steven and Lewis, 2003, for example). For high speed flight and at high altitudes the Earth radius and rotation can significantly alter the flight mechanics, and must be considered within the equations of motion, as shown in the work of Austin (2002).

The first step to simulate a flight is to trim the aircraft. In longitudinal flight, trimming means finding the angle of attack, thrust and elevator deflection that solves the system of equations described in Eq. (15) (Austin, 2002). These equations, written in the body reference frame, represent the equilibrium conditions for both rotating and non-rotating Earth, the difference being simply the Earth rotation value.

ISSN 2176-5480

$$\begin{aligned}(F_x - mg\sin\theta)/m \; - (q + q_B^E)w + (r + r_B^E)v = 0\\ (F_z - mg\cos\theta\cos\phi)/m \; - (p + p_B^E)v + (q + q_B^E)u = 0\\ M - r\,(I_{xx}\,p + I_{xz}\,r) + p\,(I_{xz}\,p + I_{zz}\,r) = 0\end{aligned} \tag{15}$$

Where F represents the aircraft aeropropulsive forces, I the moments of inertia and p_B^E, q_B^E, r_B^E are the angular velocity components associated with the Earth's rotation, explained in details further below.

In this first study, the SCRAMJET engine is not explored, and for the aircraft trimming the thrust is assumed to be exactly enough to balance the aircraft Drag.

The flight dynamics equations for a spherical, rotating Earth are listed below in Eqs. (16) to (21) (Austin, 2002).

$$\begin{aligned}\dot{u} &= (F_x - mg\sin\theta)/m \; - (q + q_B^E)w + (r + r_B^E)v\\ \dot{v} &= (F_y - mg\cos\theta\sin\phi)/m \; - (r + r_B^E)u + (p + p_B^E)w\\ \dot{w} &= (F_z - mg\cos\theta\cos\phi)/m \; - (p + p_B^E)v + (q + q_B^E)u\end{aligned} \tag{16}$$

$$\begin{aligned}\dot{p} &= \left(R + \left(I_y - I_z\right)qr\right) / I_x\\ \dot{q} &= (M + (I_z - I_x)rp) / I_y\\ \dot{r} &= \left(N + \left(I_x - I_y\right)pq\right) / I_z\end{aligned} \tag{17}$$

$$\begin{bmatrix}P\\Q\\R\end{bmatrix} = \begin{bmatrix}p\\q\\r\end{bmatrix} - L_{BV}\begin{bmatrix}\left(\omega^E + \dot{\lambda}\right)\cos\mu\\ -\dot{\mu}\\ -\left(\omega^E + \dot{\lambda}\right)\sin\mu\end{bmatrix} \tag{18}$$

$$\begin{bmatrix}\dot{\phi}\\ \dot{\theta}\\ \dot{\psi}\end{bmatrix} = \begin{bmatrix}1 & \sin\phi\tan\theta & \cos\phi\tan\theta\\ 0 & \cos\phi & -\sin\phi\\ 0 & \sin\phi\sec\theta & \cos\phi\sec\theta\end{bmatrix}\begin{bmatrix}P\\Q\\R\end{bmatrix} \tag{19}$$

$$\begin{bmatrix}\dot{x}_N\\ \dot{x}_E\\ \dot{x}_D\end{bmatrix} = L_{VB}\begin{bmatrix}u\\v\\w\end{bmatrix} \tag{20}$$

$$\begin{aligned}\dot{\mu} &= \frac{\dot{x}_N}{\mathcal{R}}\\ \dot{\lambda} &= \frac{\dot{x}_E}{\mathcal{R}\cos\mu}\end{aligned} \tag{21}$$

Where $\mathcal{R}$ is the Earth radius and L_{BV} and p_B^E, q_B^E, r_B^E are the vehicle carried vertical frame to body frame rotation and the angular velocity components associated with the Earth's rotation (ω^E), respectively, and are given by Eqs. (22) and (23).

$$L_{BV} = \begin{bmatrix}\cos\theta\cos\psi & \cos\theta\sin\psi & -\sin\theta\\ \sin\phi\sin\theta\cos\psi - \cos\phi\sin\psi & \sin\phi\sin\theta\sin\psi + \cos\phi\cos\psi & \sin\phi\cos\theta\\ \cos\phi\sin\theta\cos\psi + \sin\phi\sin\psi & \cos\phi\sin\theta\sin\psi - \sin\phi\cos\psi & \cos\phi\cos\theta\end{bmatrix} \tag{22}$$

$$\begin{bmatrix}p_B^E\\ q_B^E\\ r_B^E\end{bmatrix} = L_{BV}\begin{bmatrix}\cos\mu\\0\\-\sin\mu\end{bmatrix}\omega^E \tag{23}$$

3. RESULTS AND DISCUSSION

3.1 Airframe mathematical model

The mathematical model of the test vehicle airframe was obtained using supersonic flow equations assuming a calorically perfect gas, as discussed in the previous section, implemented in MATLAB® language.

To verify the consistency of the results, a well-known CFD program (ANSYS Fluent) was used to generate pressure results on the surfaces of a similar model, with this same model being used as input to the programmed MATLAB® routine. For the CFD run inviscid, calorically perfect gas was assumed. Figure 2 shows the result comparison for three different angles of attack, with flow conditions of Mach 7 at an altitude of 30 km.

ISSN 2176-5480

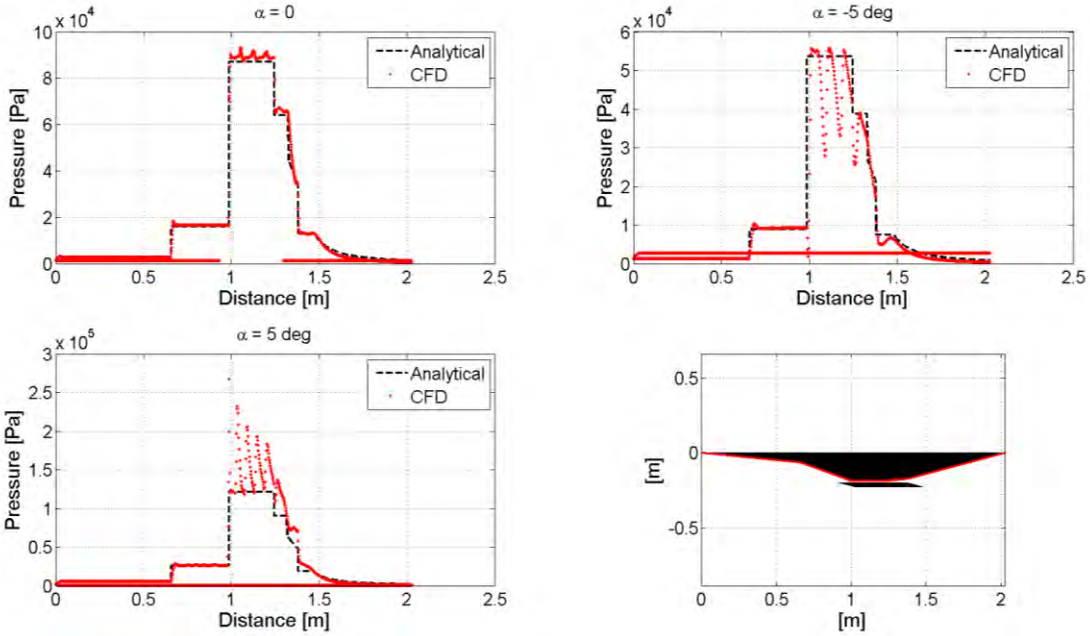

Figure 2. CFD and MATLAB® results comparison

Within the MATLAB® script, pressure distribution along the vehicle surface was used to determine forces and moment at its center of mass, hence calculating the vehicle aerodynamic coefficients. These coefficients were obtained for several angles of attack and Mach numbers, in order to produce polynomial interpolations of the coefficients as functions of such variables. Figure 3 shows the variation of the Moment Coefficient with Mach number and angle of attack, as an example.

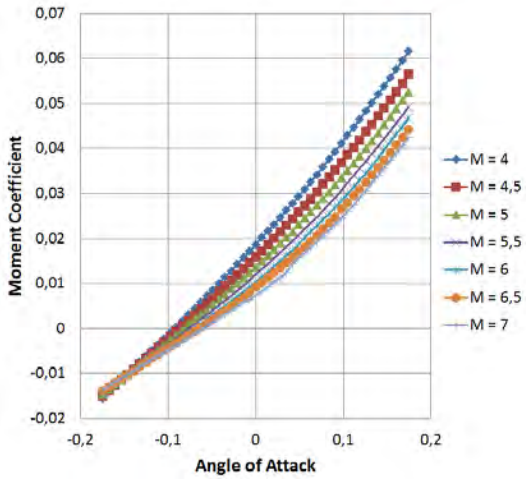

Figure 3. Moment Coefficient as a function of Mach number and angle of attack

With these curves, it is possible to have a polynomial equation such that the aerodynamic coefficient of interest (for example Moment Coefficient) is given by Eq. (24), which in turn has polynomial coefficients given by Eq. (25), with constant a and b, hence accounting for the contributions of both the angle of attack and the Mach number.

$$CM = c_2\alpha^2 + c_1\alpha + c_0 \tag{24}$$

$$c_i = aM + b \tag{25}$$

Each polynomial degree was defined as the minimum needed to best describe the behavior of the respective aerodynamic or polynomial coefficient. For Moment and Drag, a second order polynomial was enough, whilst for the Lift Coefficient a third order polynomial was needed. The polynomial interpolation of the coefficients c_i was always of first order for the airframe.

ISSN 2176-5480

3.2 Horizontal tail design

As Fig. 3 shows, the vehicle airframe presents a positive variation of Moment Coefficient with increase of the angle of attack, being inherently unstable in flight. Adequate control surfaces must be designed. In this first study, free-flight is considered, meaning that no active control is present. Hence the control surface must present a Lift Coefficient variation such that the aircraft final Moment Coefficient variation is negative with respect to the angle of attack.

Assuming small angles of attack and rear wing deflection, the minimum Lift Coefficient variation can be easily found as Eq. (26).

$$\frac{dCL_{ctr}}{d\alpha} = \frac{dCM}{d\alpha} \; \frac{S\,c}{2\,S_{ctr}\,\Delta x} \tag{26}$$

Where α is the angle of attack, S represents area, c the vehicle chord, Δx the horizontal distance between the horizontal tail center of pressure and the aircraft center of mass, and the subscript *crl* denotes the control surface.

Symmetric and asymmetric diamond-shaped airfoils were considered, with maximum thickness and maximum thickness position to be defined, as shown in Fig. 4.

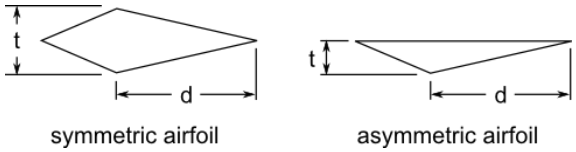

Figure 4. Diamond-shaped airfoils

A Design of Experiments approach was considered in order to verify the influence of each parameter on two important aerodynamic properties, namely the resulting Lift Coefficient variation with angle of attack and the Drag Coefficient order of magnitude.

Fixing the airfoil chord, the airfoil maximum thickness and its position on the chord were varied from 5% to 40% of the chord and from 30% to 70% of the chord, respectively, and parasite Drag Coefficient and approximated Lift Coefficient variation with angle of attack were stored for each configuration.

As shown in Eq. (26), a few geometric parameters of the horizontal tail must be defined in order to calculate the minimum required $dCL/d\alpha$ and proceed to the tradeoff analysis. It is thus admitted that each elevator should have no more than 0,6 m chord and 0,3 m span, and their center of pressure is located at approximately 0,6 m from the aircraft center of mass.

Figure 5 shows the resulting data acquired from the Design of Experiments simulation, along with a horizontal surface representing the minimum $dCL/d\alpha$ calculated at the specified conditions. For a more direct comparison, the asymmetric airfoil is assumed to be half the symmetric one, thus having thickness *t/2* (half the value exhibited on the thickness axis).

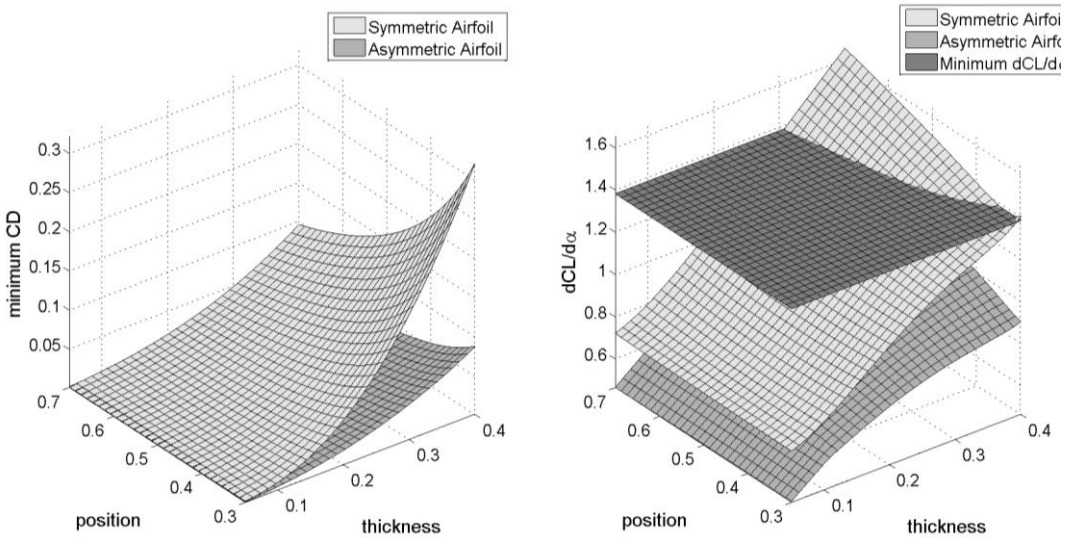

Figure 5. Design of Experiments results

ISSN 2176-5480

The Design of Experiments shows that, although the asymmetric airfoil presents significantly less Drag (combined with more Lift, not shown), this type of geometry is not capable of generating a high enough $dCL/d\alpha$. Among the symmetrical configurations, the ones with higher thickness are able to provide the required $dCL/d\alpha$, and moving the maximum thickness aft decreases parasite Drag.

Accounting for the inaccuracies due to simplifications adopted in the inferior threshold determination, an airfoil of 34% thickness at 60% of the leading edge was chosen.

A polynomial representation of the aerodynamic coefficients of this airfoil was obtained following a procedure similar to the one used previously for the airframe, with a MATLAB® script. In this case, however, the Lift Coefficient is reasonably represented only when using a third order polynomial in angle of attack (analogous to Eq. (24)), and second order polynomial in Mach number (the case of Eq. (25)). For the Drag Coefficient, second order polynomial in angle of attack was enough, but second order polynomial in Mach number was still required.

Figure 6 shows the Moment Coefficient variation with angle of attack of the vehicle without horizontal tail (airframe only) and with the chosen horizontal tail locked at 0º deflection. It can be seen that the designed horizontal tail is able to oppose the negative airframe Moment Coefficient variation, such that dynamically stable free-flight becomes possible.

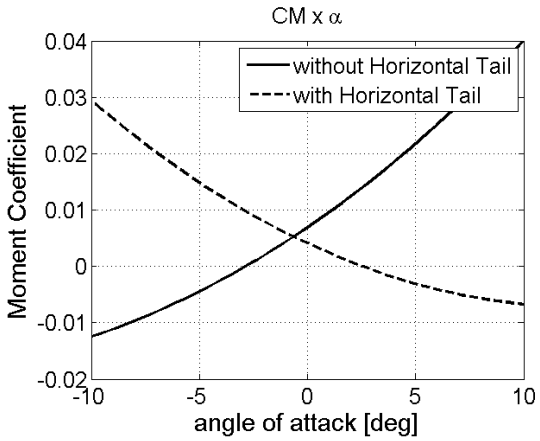

Figure 6. Moment Coefficient variation with angle of attack of the aircraft with and without horizontal tail

3.3 Flight simulation

As it was mentioned in the previous sections, free-flight is analyzed. Therefore, once trimmed, the horizontal tail is locked at its trimmed position. Positive angles of attack are expected, as when simplifying the 14-X into a bidimensional airframe a large portion of lifting surfaces are discarded. The same can be said about trailing edge down elevator, as the 14-XB presented largely positive moment coefficient.

In this first study, SCRAMJET operation is not being considered, as a working SCRAMJET greatly modifies the pressure distribution along several surfaces of the aircraft, changing entirely its dynamic behavior. Instead, it is assumed that a constant thrust booster is coupled to the vehicle, generating enough thrust to compensate for the aircraft drag.

Several cases were studied, all starting at zero latitude and longitude, altitude of 30 km and at Mach number 7. The test series aims at obtaining a first estimate of the aircraft dynamic behavior and studying the effects of different Earth model considerations on the vehicle, namely: flat Earth; spherical, non-rotating Earth; and finally spherical, rotating Earth.

For the flat Earth model, a trimmed flight heading north was simulated. Trimming yielded angle of attack of 2.41°, elevator deflection of 1.267° with trailing edge down and 2062 N thrust. Figure 7 shows the flight simulation results. A perfectly compensated flight can be observed. In order to verify flight stability, however, this case is not enough. It merely shows that the designed horizontal tail is indeed capable of compensating the airframe strong positive moment, allowing for a horizontal flight.

Another flight with flat Earth model was simulated, forcing a disturbance of 1° trailing edge down on the elevator for the first 2 seconds of flight and then returned to the trimmed position. Figure 8 shows the results. Two very distinct dynamic modes can be seen. There is a short-period mode which is stable and lightly damped, and a phugoid mode that appears to be unstable. These modes will be discussed in more details further below.

ISSN 2176-5480

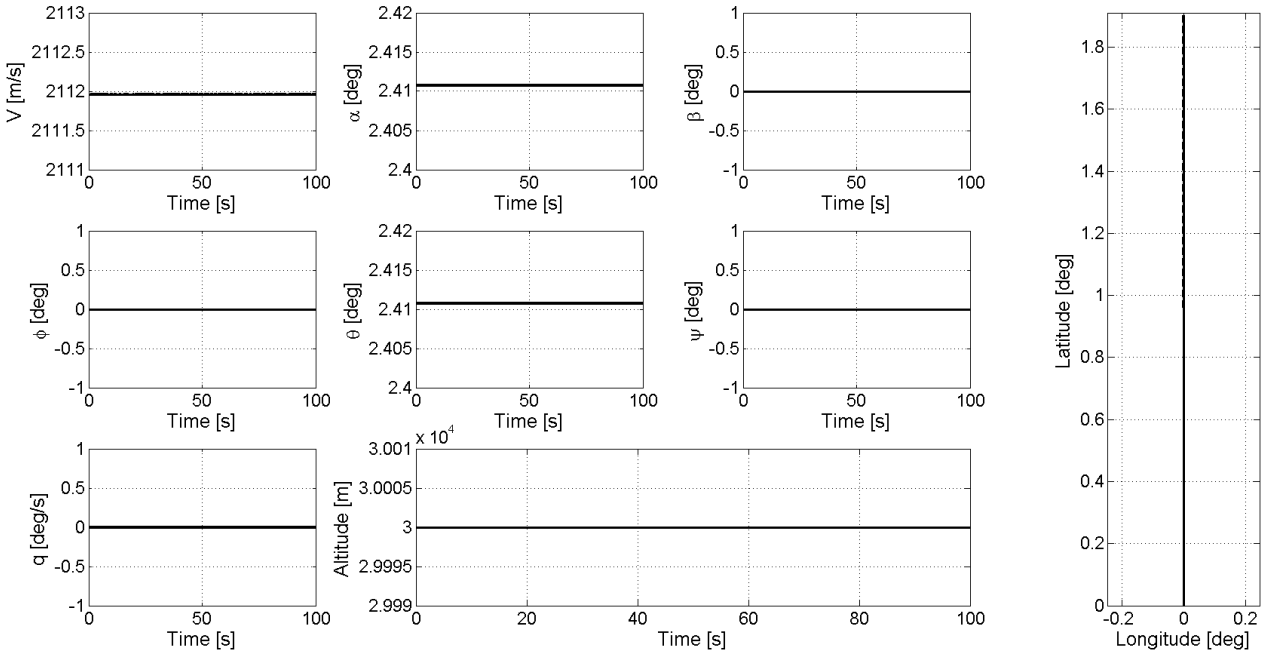

Figure 7. Flight simulation results for a Flat Earth model

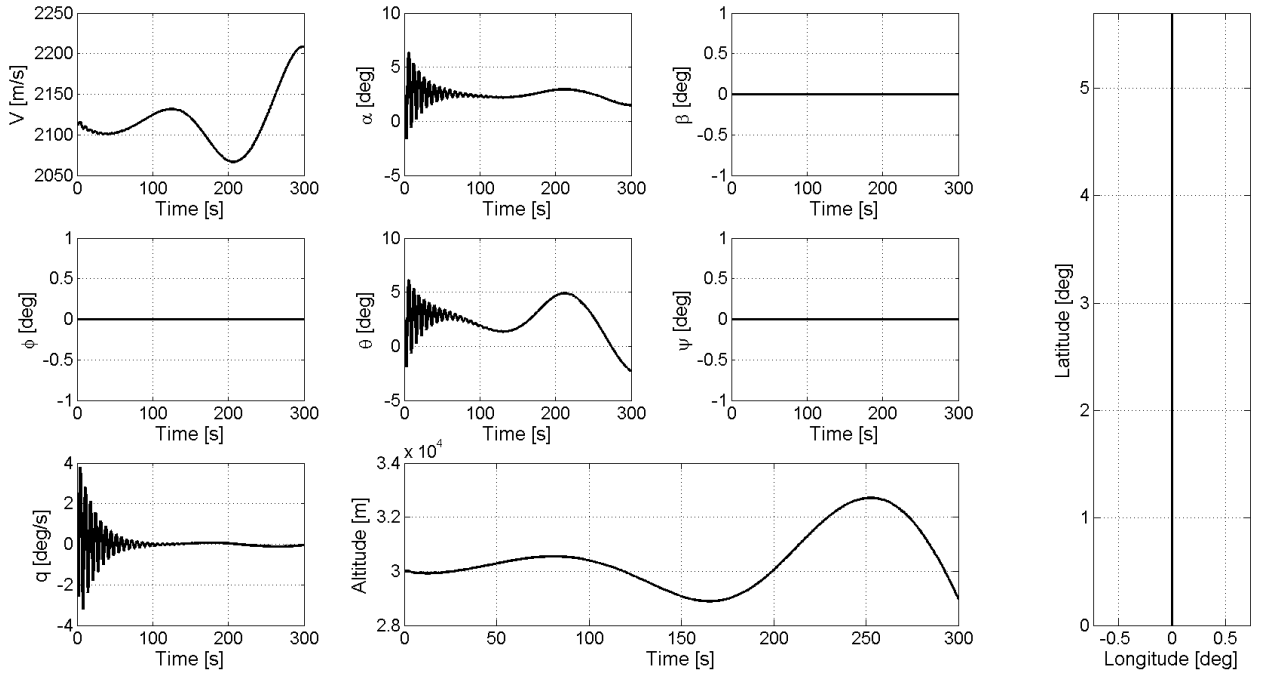

Figure 8. Flight simulation results for a flat Earth model with forced disturbance

Now, the spherical Earth is considered, first neglecting the Earth's rotation. The aircraft trimming is not affected by the Earth's sphericity, and the trimmed angle of attack, elevator deflection and thrust for a horizontal flight at the mentioned conditions are still 2.41°, 1.267° trailing edge down and 2062 N, respectively.

Figure 9 shows the flight simulation results for a trimmed flight headed north, with no forced disturbances assumed. It is quite clear the similarity of these results with those of Fig. 8, again an unstable phugoid mode being observed, even though flight was trimmed and no disturbances were forced on the aircraft.

ISSN 2176-5480

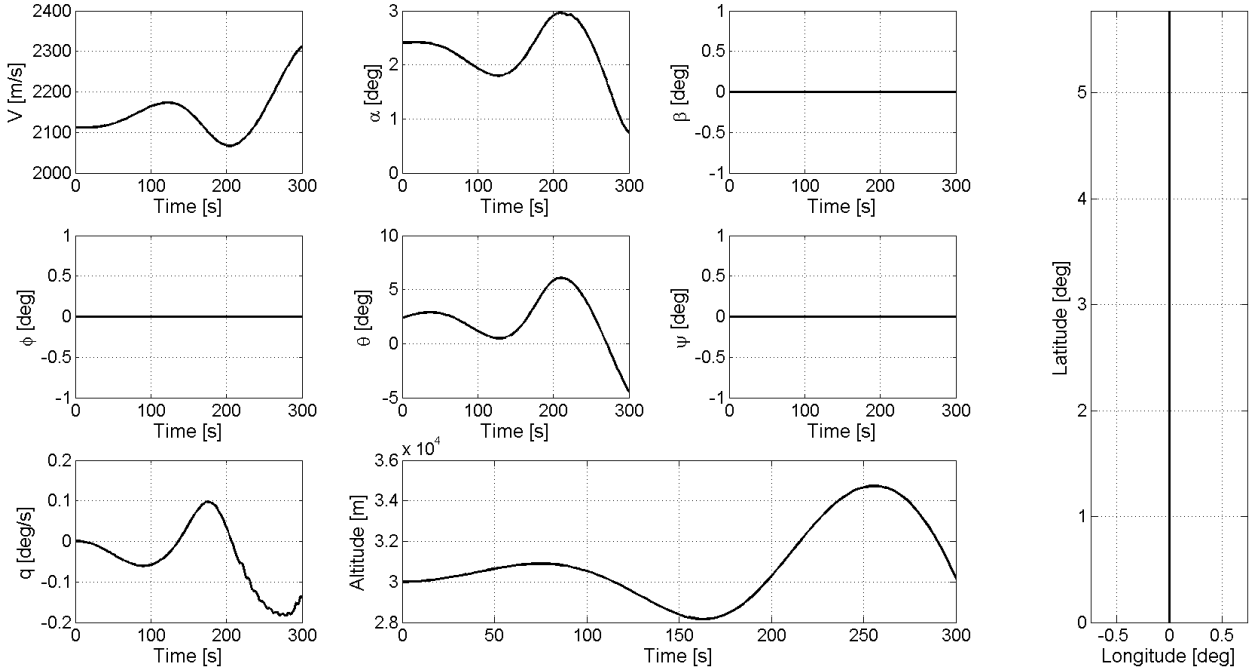

Figure 9. Flight simulation results for a spherical, non-rotating Earth model

Figure 10 helps to understand what happened when a spherical Earth was considered. At the initial time, the aircraft is leveled and presents well defined speed, angle of attack and altitude, such as to fly horizontally. Performing such flight on a spherical reference surface leads to an increase of the pitch angle, as the vehicle carried vertical frame rotates.

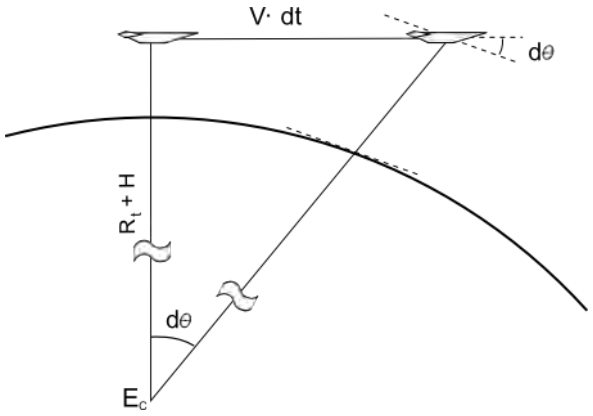

Figure 10. Flight on a Spherical Earth

This effect is expressed in the equations of motion in Eq. (18). It is more noticeable as the latitude and longitude derivatives are bigger, such as in the case of hypersonic flight.

Returning to Fig. 9, it can be seen that speed, angle of attack and altitude are constant at the beginning of the flight simulation, and pitch rate is zero. Also, all of them present a zero derivative in the first seconds. This confirms that the aircraft is trimmed. However, the pitch angle varies right from the start, as Fig. 10 shows, and this eventually induces the other state variables to change. With the dynamic instability previously observed, the pitch angle variation is much more evident, and leads to an unstable flight.

It should be noticed that it is possible to determine a pitch rate such as to force the aircraft to maintain a constant pitch angle when flying on a spherical Earth. Referring to Fig. 10, this pitch rate can be determined as Eq. (27).

$$q = -\operatorname{atan}\left(\frac{V}{R_t+H}\right) \tag{27}$$

With effect, Fig. 11 shows the results of a flight simulation using spherical, non-rotating Earth, trimmed for horizontal flight but forcing the mentioned pitch rate.

ISSN 2176-5480

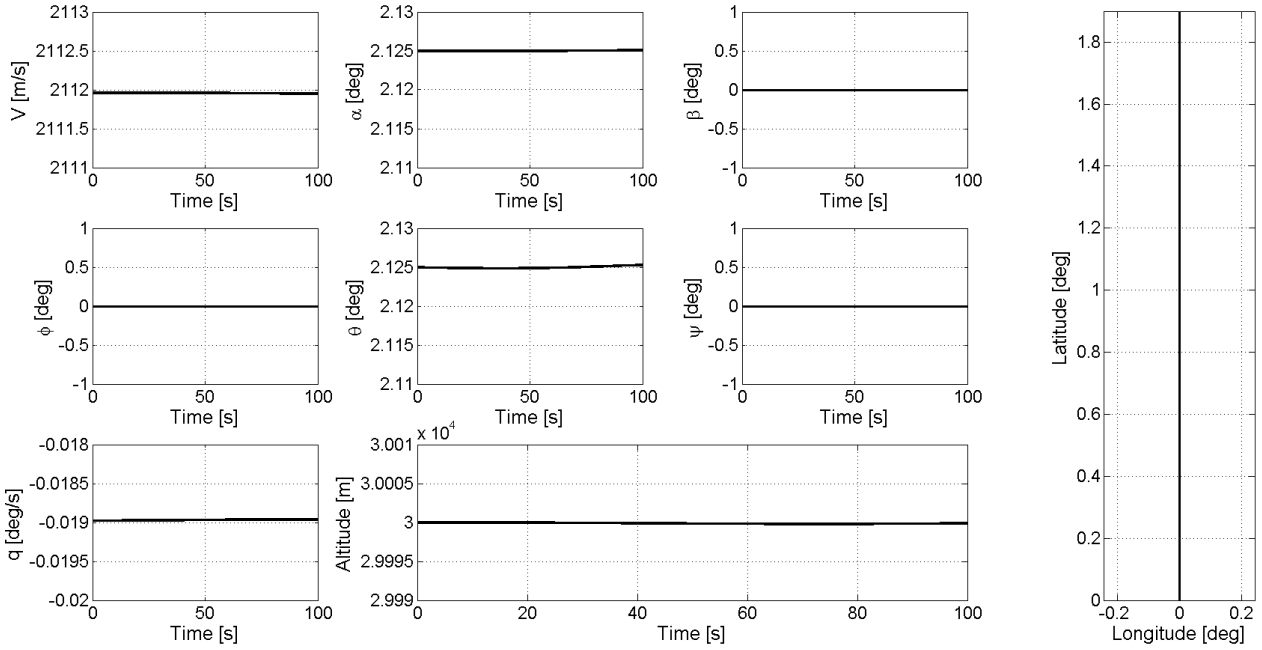

Figure 11. Flight simulation results for a spherical, non-rotating Earth model with pitch rate adjust

In order to achieve a trimmed horizontal flight with non-zero pitch rate calculated using Eq. (27), the trimmed conditions were: angle of attack 2.125°, elevator deflection 1.368 with trailing edge down and 2010 N thrust.

These results, however, do not overcome the fact that the vehicle is unstable. Simulating long enough or slightly varying the calculated pitch rate will still result in an unstable flight. A stable aircraft should not need the forced pitch rate to achieve a stabilized flight. This forced pitch rate will not be considered for the next simulations.

Finally, the effects of a spherical, rotating Earth are analyzed. First, a flight heading north is simulated. Figure 12 shows the flight simulation results. Both non-rotating and rotating Earth models yielded the same trimmed conditions, namely angle of attack 2.411°, elevator deflection 1.267° trailing edge down and 2062 N thrust, same results as those obtained for the first cases.

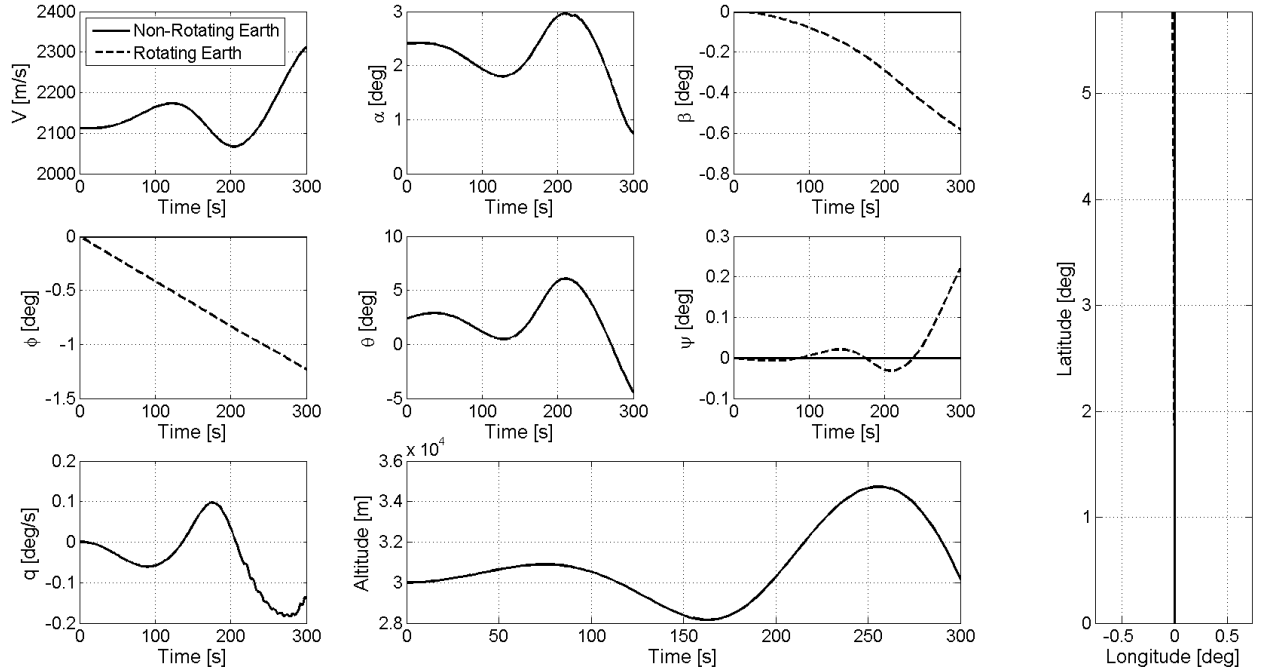

Figure 12. Flight simulation results for a spherical, rotating Earth model, vehicle heading north

ISSN 2176-5480

It can be seen that the Earth's rotation induces some lateral movement, such as sideslip angle and roll angle, which cannot be compensated due to the vehicle's lack of lateral movement control surfaces.

On the other hand, longitudinal movement is little or not affected at all by the Earth's rotation in this case. To better assess the Earth's rotation influence on the dynamic modes, the aircraft models of non-rotating and rotating Earth were linearized around the trimmed conditions for each case and the A matrix eigenvalues were analyzed. Table 1 presents the longitudinal modes eigenvalues for each case. It can be seen that when flying north the Earth's rotation presents insignificant influence on the longitudinal dynamic modes.

Table 1. Eigenvalues and dynamic modes for north headed flight.

	Eigenvalue	Mode	Period [s]	Damping Ratio
Non-rotating Earth	-0.04271 ± 0.9473 i	Short-Period	6.63	0.0450
	0.009211 ± 0.03706 i	Phugoid	169.5	-0.2412
Rotating Earth	-0.04271 ± 0.9473 i	Short-Period	6.63	0.0450
	0.009210 ± 0.03706 i	Phugoid	169.5	-0.2412

Next, a flight headed east is analyzed. Figure 13 shows the simulation results. For this flight condition, non-rotating Earth model yielded the same trimming conditions as before, as expected, while rotating Earth model yielded angle of attack 2.348°, elevator deflection 1.289° trailing edge down and 2050 N thrust.

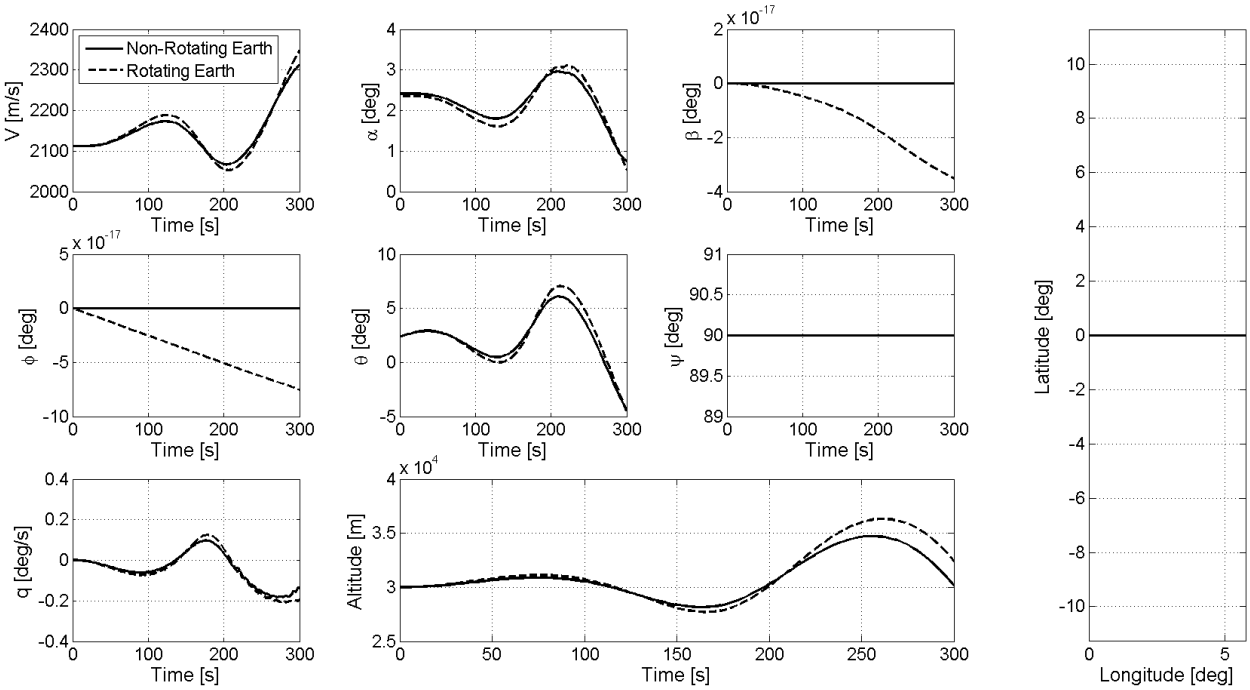

Figure 13. Flight simulation results for a spherical, rotating Earth model, vehicle heading east

In this case, lateral movement is negligible. Looking at the longitudinal movement, however, the Earth's rotation appears to have increased the destabilizing movement. Again, the A matrix longitudinal modes eigenvalues are analyzed, presented in Table 2.

Table 2. Eigenvalues and dynamic modes for east headed flight.

	Eigenvalue	Mode	Period [s]	Damping Ratio
Non-rotating Earth	-0.04271 ± 0.9473 i	Short-Period	6.63	0.0450
	0.009211 ± 0.03706 i	Phugoid	169.5	-0.2412
Rotating Earth	-0.04258 ± 0.9501 i	Short-Period	6.61	0.0448
	0.009167 ± 0.03681 i	Phugoid	170.7	-0.2416

ISSN 2176-5480

In fact, although very subtle in this case, the Earth's rotation did have a negative effect on the dynamic modes, slightly decreasing the damping ratio of the short-period mode and increasing the instability of the phugoid mode. The modes periods were also lightly changed, having increased for the unstable mode and decreased for the stable mode.

For last, a flight headed west is analyzed. Figure 14 shows the simulation results. For this last simulation, non-rotating Earth model once again yielded the same trimming conditions as before, while rotating Earth model now yielded angle of attack 2.473°, elevator deflection 1.245° trailing edge down and 2074 N thrust.

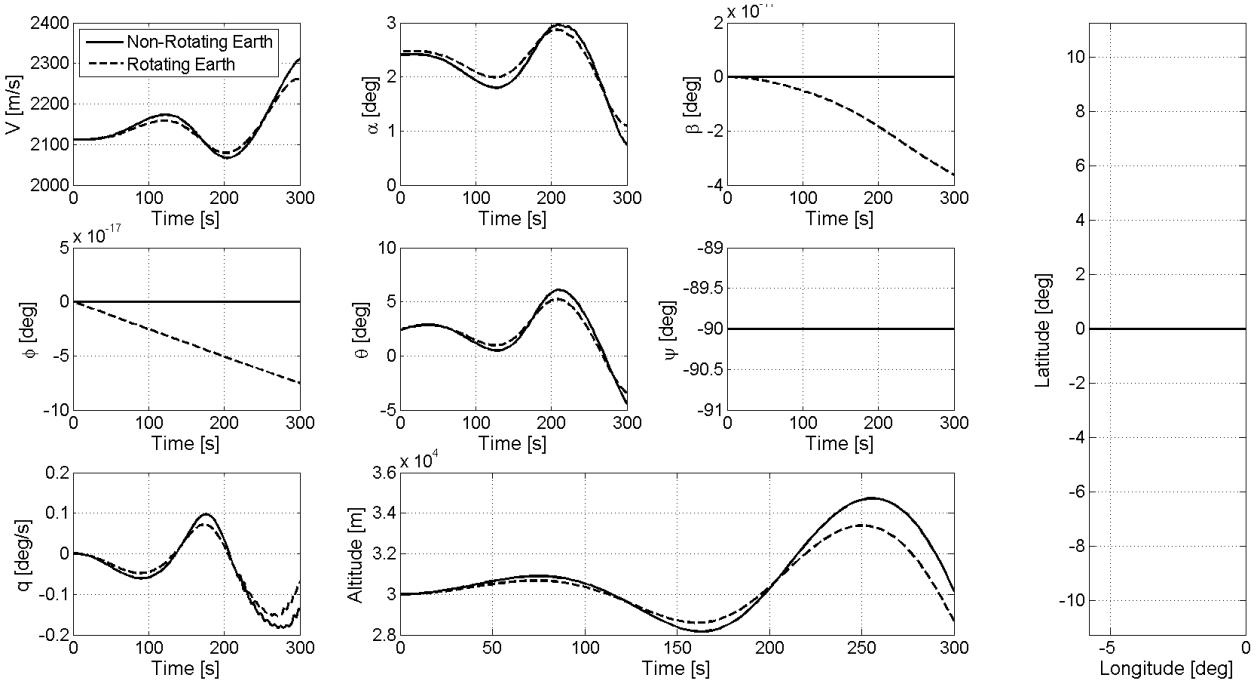

Figure 14. Flight simulation results for a spherical, rotating Earth model, vehicle heading west

Lateral movement is once again negligible, and in this case the Earth's rotation seems to have lessened the aircraft unstable longitudinal dynamics effects. Table 3 presents the longitudinal modes eigenvalues for this case.

Table 3. Eigenvalues and dynamic modes for west headed flight.

	Eigenvalue	Mode	Period [s]	Damping Ratio
Non-rotating Earth	-0.04271 ± 0.9473 i	Short-Period	6.63	0.0450
	0.009211 ± 0.03706 i	Phugoid	169.5	-0.2412
Rotating Earth	-0.04284 ± 0.9446 i	Short-Period	6.65	0.0453
	0.009256 ± 0.03731 i	Phugoid	168.4	-0.2408

Again it is very subtle, but the Earth's rotation now contributes in the direction of stabilizing the aircraft, having increased the short-period damping ratio and decreased the phugoid instability. Period change was also reversed, having increased for the stable mode and decreased for the unstable mode.

4. CONCLUDING REMARKS

This paper presented an initial stability study of the 14-X Airspace Hypersonic Vehicle, currently under development at the Institute for Advanced Studies (IEAv/DCTA). A bidimensional simplification of such aircraft, the 14-XB, was used in this initial study.

The equations and hypotheses adopted to produce a mathematical model that adequately represents the vehicle aerodynamics were presented in detail. An all-moving horizontal tail was designed, in order to compensate the highly positive airframe Moment Coefficient variation with angle of attack.

The all-moving horizontal tail was locked at trimmed position and a few horizontal flight cases of interest were simulated considering the presence of the Earth's rotation and sphericity in the rigid-body movement equations, aiming at better understanding the free-flight dynamics of the 14-XB and the effects of a spherical, rotating Earth on a hypersonic, high-altitude flight.

ISSN 2176-5480

Flight simulation results showed that the designed horizontal tail was capable of trimming the aircraft. However, the longitudinal dynamics of the vehicle was analyzed using flight simulation and eigenvalue study, and the aircraft presented a stable, lightly damped short-period mode and an unstable phugoid mode. The Earth's sphericity represented a disturbance to the trimmed aircraft, hence leading to an unstable flight. Finally, simulation results and eigenvalue analysis showed that the Earth's rotation can increase, decrease or have no effect on destabilizing issues, depending on the vehicle trajectory.

Future works will focus on designing an active controller to solve the 14-XB stability issue observed in this work.

5. REFERENCES

Anderson, J.D., 1990. *Modern Compressible Flow: with historical perspective*. McGraw-Hill, USA, 2nd edition.

Austin, K.J., 2002. *Evolutionary Design of Robust Flight Control for a Hypersonic Aircraft*. Ph.D. thesis, The University of Queensland, Australia.

Frendreis, S.G.V., Torstens, S. and Cesnik, C.E.S., 2009. "Six-Degree-of-Freedom Simulation of Hypersonic Vehicles". In *Proceedings of AIAA Atmospheric Flight Mechanics Conference.* Chicago, USA.

Heiser, W.H. and Pratt, D.T., 1994. *Hypersonic Airbreathing Propulsion*. American Institute of Aeronautics and Astronautics, Washington DC.

Rolim, T.C., 2009. *Experimental Analysis of a Hypersonic Waverider*. M.Sc. thesis, Aeronautics Institute of Technology, Brazil.

Stevens, B.L. and Lewis, F.L., 2003. *Aircraft Control and Simulation*. John Wiley & Sons, New Jersey, 2nd edition.

6. RESPONSIBILITY NOTICE

The authors are the only responsible for the printed material included in this paper.